



Violation of the Cauchy-Schwarz Inequality with Matter Waves

K. V. Kheruntsyan,¹ J.-C. Jaskula,^{2,*} P. Deuar,³ M. Bonneau,² G. B. Partridge,^{2,†} J. Ruudel,² R. Lopes,² D. Boiron,² and C. I. Westbrook²

¹The University of Queensland, School of Mathematics and Physics, Brisbane, Queensland 4072, Australia

²Laboratoire Charles Fabry de l'Institut d'Optique, CNRS, Université Paris-Sud,
Campus Polytechnique RD128, 91127 Palaiseau, France

³Institute of Physics, Polish Academy of Sciences, Al. Lotników 32/46, 02-668 Warsaw, Poland

(Received 30 March 2012; published 25 June 2012)

The Cauchy-Schwarz (CS) inequality—one of the most widely used and important inequalities in mathematics—can be formulated as an upper bound to the strength of correlations between classically fluctuating quantities. Quantum-mechanical correlations can, however, exceed classical bounds. Here we realize four-wave mixing of atomic matter waves using colliding Bose-Einstein condensates, and demonstrate the violation of a multimode CS inequality for atom number correlations in opposite zones of the collision halo. The correlated atoms have large spatial separations and therefore open new opportunities for extending fundamental quantum-nonlocality tests to ensembles of massive particles.

DOI: [10.1103/PhysRevLett.108.260401](https://doi.org/10.1103/PhysRevLett.108.260401)

PACS numbers: 03.75.Be, 03.75.Gg, 34.50.Cx, 42.50.Dv

The Cauchy-Schwarz (CS) inequality is ubiquitous in mathematics and physics [1]. Its utility ranges from proofs of basic theorems in linear algebra to the derivation of the Heisenberg uncertainty principle. In its basic form, the CS inequality simply states that the absolute value of the inner product of two vectors cannot be larger than the product of their lengths. In probability theory and classical physics, the CS inequality can be applied to fluctuating quantities and states that the expectation value of the cross correlation $\langle I_1 I_2 \rangle$ between two quantities I_1 and I_2 is bounded from above by the autocorrelations in each quantity,

$$|\langle I_1 I_2 \rangle| \leq \sqrt{\langle I_1^2 \rangle \langle I_2^2 \rangle}. \quad (1)$$

This inequality is satisfied, for example, by two classical currents emanating from a common source.

In quantum mechanics, correlations can, however, be stronger than those allowed by the CS inequality [2–4]. Such correlations have been demonstrated in quantum optics using, for example, antibunched photons produced via spontaneous emission [5], or twin photon beams generated in a radiative cascade [6], parametric down conversion [7], and optical four-wave mixing [8]. Here the discrete nature of the light and the strong correlation (or anticorrelation in antibunching) between photons is responsible for the violation of the CS inequality. The violation has even been demonstrated for two light beams detected as continuous variables [8].

In this work we demonstrate a violation of the CS inequality in matter-wave optics using pair-correlated atoms formed in a collision of two Bose-Einstein condensates (BECs) of metastable helium [9–12] (see Fig. 1). The CS inequality which we study is a *multimode* inequality, involving integrated atomic densities, and therefore is different from the typical two-mode situation studied in

quantum optics. Our results demonstrate the potential of atom optics experiments to extend the fundamental tests of quantum mechanics to ensembles of massive particles. Indeed, violation of the CS inequality implies the possibility of (but is not equivalent to) formation of quantum states that exhibit the Einstein-Podolsky-Rosen (EPR) correlations or violate a Bell's inequality [3]. The EPR and Bell-state correlations are of course of wider significance

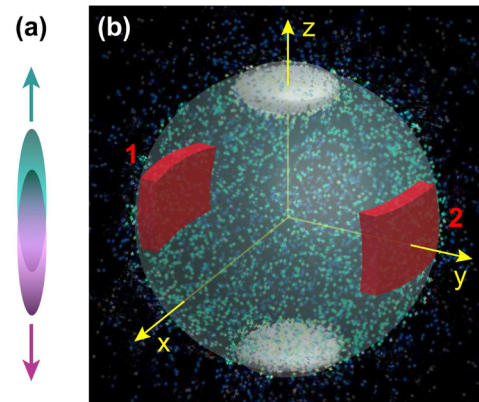


FIG. 1 (color online). Diagram of the collision geometry. (a) Two cigar-shaped condensates moving in opposite directions along the axial direction z shortly after their creation by a Bragg laser pulse (the anisotropy and spatial separation are not to scale). (b) Spherical halo of scattered atoms produced by four-wave mixing after the cloud expands and the atoms fall to the detector 46 cm below. During the flight to the detector, the unscattered condensates acquire a disk shape shown in white on the north and south poles of the halo. The (red) boxes 1 and 2 illustrate a pair of diametrically symmetric counting zones (integration volumes) for the average cross-correlation and autocorrelation functions, $\bar{G}_{12}^{(2)}$ and $\bar{G}_{ii}^{(2)}$ ($i = 1, 2$) (see text), used in the analysis of the Cauchy-Schwarz inequality.

to foundational principles of quantum mechanics than those that violate a CS inequality. Nevertheless, the importance of understanding the CS inequality in new physical regimes lies in the fact that: (i) they are the simplest possible tests of stronger-than-classical correlations, and (ii) they can be viewed as precursors, or necessary conditions, for the stricter tests of quantum mechanics.

The atom-atom correlations resulting from the collision and violating the CS inequality are measured after long time-of-flight expansion using time- and position-resolved atom detection techniques unique to metastable atoms [13]. The 307 ms long expansion time combined with a large collision and hence scattering velocity results in a ~ 6 cm spatial separation between the scattered, correlated atoms. This separation is quite large compared to what has been achieved in recent related BEC experiments based on double-well or two-component systems [14–16], trap modulation techniques [17], or spin-changing interactions [18,19]. This makes the BEC collisions ideally suited to quantum-nonlocality tests using ultracold atomic gases and the intrinsic interatomic interactions.

In a simple two-mode quantum problem, described by boson creation and annihilation operators \hat{a}_i^\dagger and \hat{a}_i ($i = 1, 2$), the Cauchy-Schwarz inequality of the form of Eq. (1) can be formulated in terms of the second-order correlation functions, $G_{ij}^{(2)} = \langle \hat{n}_i \hat{n}_j \rangle = \langle \hat{a}_i^\dagger \hat{a}_j^\dagger \hat{a}_j \hat{a}_i \rangle$, and reads [2–4]

$$G_{12}^{(2)} \leq [G_{11}^{(2)} G_{22}^{(2)}]^{1/2}, \quad (2)$$

or simply $G_{12}^{(2)} \leq G_{11}^{(2)}$ in the symmetric case of $G_{11}^{(2)} = G_{22}^{(2)}$. Here, $G_{12}^{(2)} = G_{21}^{(2)}$, $\hat{n}_i = \hat{a}_i^\dagger \hat{a}_i$ is the particle number operator, and the double colons indicate normal ordering of the creation and annihilation operators, which ensures the correct quantum-mechanical interpretation of the process of detection of pairs of particles that contribute to the measurement of the second-order correlation function [2]. Stronger-than-classical correlation violating this inequality would require $G_{12}^{(2)} > [G_{11}^{(2)} G_{22}^{(2)}]^{1/2}$, or $G_{12}^{(2)} > G_{11}^{(2)}$ in the symmetric case.

The situation we analyze here is counterintuitive in that we observe a peak cross correlation (for pairs of atoms scattered in opposite directions) that is smaller than the peak autocorrelation (for pairs of atoms propagating in the same direction). In a simple two-mode model such a ratio of the cross correlation and autocorrelation satisfies the classical CS inequality. However, in order to adequately treat the atom-atom correlations in the BEC collision problem, one must generalize the CS inequality to a multi-mode situation, which takes into account the fact that the cross correlations and autocorrelations in matter-wave optics are usually *functions* (in our case of momentum). The various correlation functions can have different widths and peak heights, and one must define an appropriate integration domain over multiple momentum modes to recover an

inequality that plays the same role as that in the two-mode case and *is* actually violated, as we show below.

The experimental setup was described in Refs. [11,12]. Briefly, a cigar-shaped BEC of metastable helium, containing approximately $\sim 10^5$ atoms, trapped initially in a harmonic trapping potential with frequencies $(\omega_x, \omega_y, \omega_z)/2\pi = (1500, 1500, 7.5)$ Hz, was split by Bragg diffraction into two parts along the axial (z -) direction [see Fig. 1(a)], with velocities differing by twice the single photon recoil velocity $v_{\text{rec}} = 9.2$ cm/s. Atoms interact via binary, momentum conserving s -wave collisions and scatter onto a nearly spherical halo [see Fig. 1(b)] whose radius in velocity space is about the recoil velocity [11,20]. The scattered atoms fall onto a detector that records the arrival times and positions of individual atoms [13] with a quantum efficiency of $\sim 10\%$. The halo diameter in position space at the detector is ~ 6 cm. We use the arrival times and positions to reconstruct three-dimensional velocity vectors \mathbf{v} for each atom. The unscattered BECs locally saturate the detector. To quantify the strength of correlations corresponding only to spontaneously scattered atoms, we exclude from the analysis the data points containing the BECs and their immediate vicinity ($|v_z| < 0.5v_{\text{rec}}$) and further restrict ourselves to a spherical shell of radial thickness $0.9 < v_r/v_{\text{rec}} < 1.1$ (where the signal to noise is large enough), defining the total volume of the analyzed region as $\mathcal{V}_{\text{data}}$.

Using the atom arrival and position data, we can measure the second-order correlation functions between the atom number densities $\hat{n}(\mathbf{k})$ at two points in momentum space, $\mathcal{G}^{(2)}(\mathbf{k}, \mathbf{k}') = \langle \hat{n}(\mathbf{k}) \hat{n}(\mathbf{k}') \rangle$ (see Supplementary Material [21]), with \mathbf{k} denoting the wave vector $\mathbf{k} = m\mathbf{v}/\hbar$ and $\hbar\mathbf{k}$ the momentum. The correlation measurements are averaged over a certain counting zone (integration volume \mathcal{V}) on the scattering sphere in order to get statistically significant results. By choosing \mathbf{k}' to be nearly opposite or nearly collinear to \mathbf{k} , we can define the averaged back-to-back (BB) or collinear (CL) correlation functions,

$$\mathcal{G}_{\text{BB}}^{(2)}(\Delta\mathbf{k}) = \int_{\mathcal{V}} d^3\mathbf{k} \mathcal{G}^{(2)}(\mathbf{k}, -\mathbf{k} + \Delta\mathbf{k}), \quad (3)$$

$$\mathcal{G}_{\text{CL}}^{(2)}(\Delta\mathbf{k}) = \int_{\mathcal{V}} d^3\mathbf{k} \mathcal{G}^{(2)}(\mathbf{k}, \mathbf{k} + \Delta\mathbf{k}), \quad (4)$$

which play a role analogous to the cross-correlation and autocorrelation functions, $G_{12}^{(2)}$ and $G_{ii}^{(2)}$, in the simple two-mode problem discussed above. The BB and CL correlations are defined as functions of the relative displacement $\Delta\mathbf{k}$, while the dependence on \mathbf{k} is lost due to the averaging.

The normalized BB and CL correlations functions, $g_{\text{BB}}^{(2)}(\Delta\mathbf{k})$ and $g_{\text{CL}}^{(2)}(\Delta\mathbf{k})$, averaged over the unexcised part of the scattering sphere $\mathcal{V}_{\text{data}}$ are shown in Fig. 2. The BB correlation peak results from binary, elastic collisions between atoms, whereas the CL correlation peak is a variant

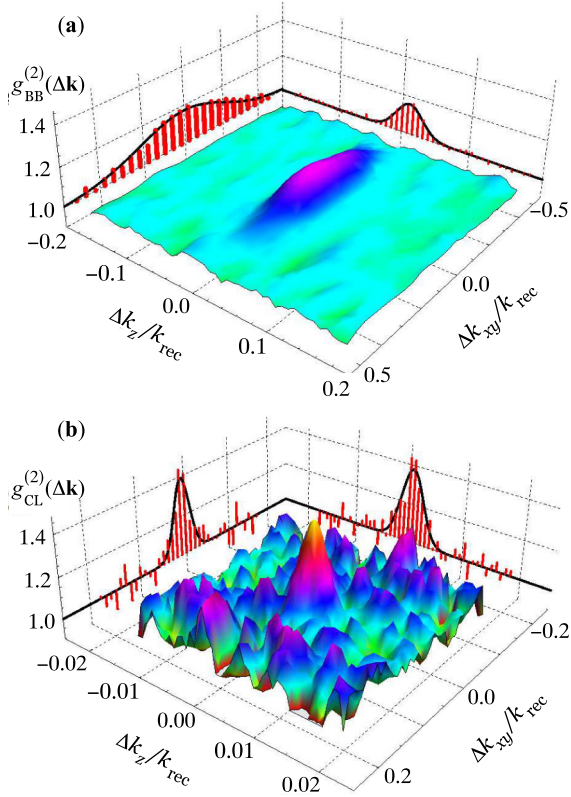


FIG. 2 (color online). Normalized back-to-back (a) and collinear (b) correlation functions, $g_{\text{BB}}^{(2)}(\Delta\mathbf{k})$ and $g_{\text{CL}}^{(2)}(\Delta\mathbf{k})$, in momentum space integrated over $\mathcal{V}_{\text{data}}$ corresponding to $|k_z| < 0.5k_{\text{rec}}$ and $0.9 < k_r/k_{\text{rec}} < 1.1$, where $k_{\text{rec}} = mv_{\text{rec}}/\hbar$ is the recoil momentum. The data are averaged over 3600 experimental runs. Because of the cylindrical symmetry of the initial condensate and of the overall geometry of the collision, the dependence on the k_x and k_y components should physically be identical and therefore can be combined (averaged); the correlation functions can then be presented as two-dimensional surface plots on the (k_z, k_{xy}) plane. The two-dimensional plots were smoothed with a nearest neighbor running average. The data points along the k_z and k_{xy} projections (corresponding to thin slices centered at $k_{xy} = 0$ and $k_z = 0$, respectively) are not smoothed. The solid lines show the Gaussian fits to these projections. The peak height of the back-to-back correlation function is ~ 1.2 while that of the collinear correlation function is ~ 1.4 , apparently confirming the Cauchy-Schwarz inequality. The widths of the two distributions are, however, very different ($\sigma_{\text{BB},x} \approx \sigma_{\text{BB},y} \approx 0.21k_{\text{rec}}$, $\sigma_{\text{BB},z} \approx 0.019k_{\text{rec}}$, whereas $\sigma_{\text{CL},x} \approx \sigma_{\text{CL},y} \approx 0.036k_{\text{rec}}$, $\sigma_{\text{CL},z} \approx 0.002k_{\text{rec}}$) and a multimode formulation of the Cauchy-Schwarz inequality, which relates the relative volumes of the correlation functions, is violated.

of the Hanbury Brown and Twiss effect [22,23]—a two-particle interference involving members of two different atom pairs [9,10,24,25]. Both correlation functions are anisotropic because of the anisotropy of the initial colliding condensates.

An important difference with the experiment of Ref. [9] is that the geometry in the present experiment (with

vertically elongated condensates) is such that the observed widths of the correlation functions are not limited by the detector resolution. Here we now observe that the BB and CL correlations have very different widths, with the BB width being significantly larger than the CL width. This broadening is largely due to the size of the condensate in the vertical direction (~ 1 mm). The elongated nature of the cloud and the estimated temperature of ~ 200 nK also means that the condensates correspond in fact to *quasicondensates* [26] whose phase coherence length is smaller than the size of the atomic cloud. The broadening of the BB correlation due to the presence of quasicondensates will be discussed in another paper [27], but we emphasize that the CS inequality analyzed here is insensitive to the detailed broadening mechanism as it relies on integrals over correlation functions. This is one of the key points in considering the multimode CS inequality.

Since the peak of the CL correlation function corresponds to a situation in which the two atoms follow the same path, we can associate it with the autocorrelation of the momentum of the particles on the collision sphere. Similarly, the peak of the BB correlation function corresponds to two atoms following two distinct paths and therefore can be associated with the cross-correlation function between the respective momenta. Hence we realize a situation in which one is tempted to apply the CS inequality to the peak values of these correlation functions. As we see from Fig. 2, if one naively uses only the peak heights, the CS inequality is *not* violated since $g_{\text{BB}}^{(2)}(0) < g_{\text{CL}}^{(2)}(0)$ and hence $\mathcal{G}_{\text{BB}}^{(2)}(0) < \mathcal{G}_{\text{CL}}^{(2)}(0)$ due to the nearly identical normalization factors (see Supplementary Material [21]).

We can, however, construct a CS inequality that is violated if we use integrated correlation functions, $\bar{\mathcal{G}}_{ij}^{(2)}$, that correspond to atom numbers $\hat{N}_i = \int_{\mathcal{V}_i} d^3\mathbf{k} \hat{a}^\dagger(\mathbf{k})\hat{a}(\mathbf{k})$ ($i = 1, 2$) in two distinct zones on the collision halo [21],

$$\bar{\mathcal{G}}_{ij}^{(2)} = \langle : \hat{N}_i \hat{N}_j : \rangle = \int_{\mathcal{V}_i} d^3\mathbf{k} \int_{\mathcal{V}_j} d^3\mathbf{k}' \mathcal{G}^{(2)}(\mathbf{k}, \mathbf{k}'). \quad (5)$$

The choice of the two integration (zone) volumes \mathcal{V}_i and \mathcal{V}_j determines whether the $\bar{\mathcal{G}}_{ij}^{(2)}$ -function corresponds to the BB ($i \neq j$) or CL ($i = j$) correlation functions, Eqs. (3) and (4).

The CS inequality that we can now analyze for violation reads $\bar{\mathcal{G}}_{12}^{(2)} \leq [\bar{\mathcal{G}}_{11}^{(2)} \bar{\mathcal{G}}_{22}^{(2)}]^{1/2}$. To quantify the degree of violation, we introduce a correlation coefficient,

$$C = \bar{\mathcal{G}}_{12}^{(2)} / [\bar{\mathcal{G}}_{11}^{(2)} \bar{\mathcal{G}}_{22}^{(2)}]^{1/2}, \quad (6)$$

which is smaller than unity classically, but can be larger than unity for states with stronger-than-classical correlations.

In Fig. 3 we plot the correlation coefficient C determined from the data for different integration zones \mathcal{V}_1 and \mathcal{V}_2 , but always keeping the two volumes equal. When \mathcal{V}_1 and \mathcal{V}_2 correspond to diametrically opposed, correlated pairs

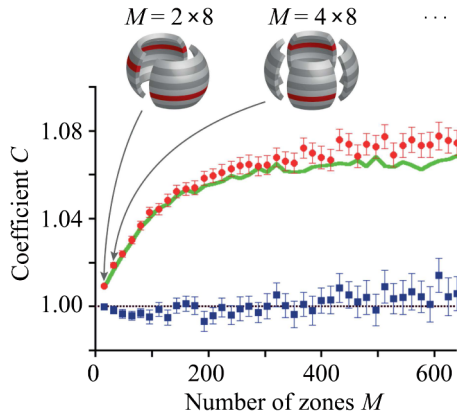


FIG. 3 (color online). Correlation coefficient C as a function of the number of zones $M = \mathcal{V}_{\text{data}}/\mathcal{V}_1$ into which we cut the scattering sphere. $C > 1$ corresponds to violation of the Cauchy-Schwarz inequality. The scattering sphere was cut into 8 polar and from 2 to 80 azimuthal zones; the resulting arrangement of zones for $M = 16$ and 32 is illustrated in the upper panel. The observed values of C for pairs of correlated diametrically opposite zones (shown as darker red stripes in the upper panel as an example) were averaged to get one data point for a given M ; the data points for such zones are shown as red circles, for uncorrelated (neighboring) zones—as blue squares. The error bars show the standard deviation of the mean over the number of zone pairs. The (green) thick solid curve is the theoretical prediction (see Supplementary Material [21]) calculated using the experimental parameters and a stochastic Bogoliubov approach [20,28].

of zones (red circles), C is greater than unity, violating the CS inequality, while for neighboring, uncorrelated pairs (blue squares) the CS inequality is not violated. The figure also shows the results of a quantum-mechanical calculation of C using a stochastic Bogoliubov approach (green thick solid curve) [20,21,28]. The calculation is for the initial total number of atoms $N = 85\,000$ and is in good agreement with the observations. The choice of large integration volumes (small number of zones M) results in only weak violations, while using smaller volumes (large M) increases the violation. This behavior is to be expected (see Supplementary Material [21]) because large integration zones include many, uncorrelated events which dilute the computed correlation. The saturation of C , in the current arrangement of integration zones—with a fixed number of polar cuts and hence a fixed zone size along z which always remains larger than the longitudinal correlation width—occurs when the tangential size of the zone begins to approach the transverse width of the CL correlation function. If the zone sizes were made smaller in all directions, we would recover the situation applicable to the peak values of the correlation functions (and hence no CS violation) as soon as the sizes become smaller than the respective correlation widths (see Eq. (S11) in the Supplementary Material [21]).

We have shown the violation of the CS inequality using the experimental data of Ref. [11] in which a sub-Poissonian variance in the atom number difference between opposite zones was observed. Although the two effects are linked mathematically in simple cases, they are not equivalent in general [8,21]. Because of the multimode nature of the four-wave mixing process, we observe stronger (weaker) suppression of the variance below the shot-noise level for the larger (smaller) zones (see Fig. 3 of [11]), whereas the degree of violation of the CS inequality follows the opposite trend. This difference can be of importance for other experimental tests of stronger-than-classical correlations in inherently multimode situations in matter-wave optics.

The nonclassical character of the observed correlations implies that the scattered atoms cannot be described by classical stochastic random variables [29]. Our experiment is an important step toward the demonstrations of increasingly restrictive types of nonlocal quantum correlations with matter waves, which we hope will one day culminate in the violation of a Bell inequality as well. In this case, the nonclassical character of correlations will also defy a description via a local hidden variable theory [4,29]. Nonoptical violations of Bell's inequalities have so far only been demonstrated for *pairs* of massive particles (such as two trapped ions [30] or proton-proton pairs in the decay of ^2He [31]), but never in the multiparticle regime. The BEC collision scheme used here is particularly well-suited for demonstrating a Bell inequality violation [32] using an atom optics analog of the Rarity-Tapster setup [33].

We thank P. Ziń and T. Wasak for useful discussions. K. V. K. is supported by the ARC FT100100285 grant, P. D. by Polish Government research grants for the years 2010–2013 and the EU contract PERG06-GA-2009-256291, J. R. by the DGA, R. L. by the FCT SFRH/BD/74352/2010, and support for the experimental work comes from the IFRAF program, the Triangle de la Physique, and the ANR grants DESINA and ProQuP.

*Current address: Harvard-Smithsonian Center for Astrophysics, Cambridge, MA 02138, USA.

†Current address: Agilent Laboratories, Santa Clara, CA 95051, USA.

- [1] J. M. Steele, *The Cauchy-Schwarz Master Class: An Introduction to the Art of Mathematical Inequalities* (Cambridge University Press, Cambridge, England, 2004).
- [2] R. J. Glauber, *Phys. Rev.* **130**, 2529 (1963).
- [3] M. D. Reid and D. F. Walls, *Phys. Rev. A* **34**, 1260 (1986).
- [4] D. F. Walls and G. J. Milburn, *Quantum Optics* (Springer-Verlag, Berlin, 2008), 2nd ed.
- [5] H. J. Kimble, M. Dagenais, and L. Mandel, *Phys. Rev. Lett.* **39**, 691 (1977).
- [6] J. F. Clauser, *Phys. Rev. D* **9**, 853 (1974).

- [7] X. Zou, L. J. Wang, and L. Mandel, *Opt. Commun.* **84**, 351 (1991).
- [8] A. M. Marino, V. Boyer, and P. D. Lett, *Phys. Rev. Lett.* **100**, 233601 (2008).
- [9] A. Perrin, H. Chang, V. Krachmalnicoff, M. Schellekens, D. Boiron, A. Aspect, and C. I. Westbrook, *Phys. Rev. Lett.* **99**, 150405 (2007).
- [10] A. Perrin, C. M. Savage, D. Boiron, V. Krachmalnicoff, C. I. Westbrook, and K. V. Kheruntsyan, *New J. Phys.* **10**, 045021 (2008).
- [11] J.-C. Jaskula, M. Bonneau, G. B. Partridge, V. Krachmalnicoff, P. Deuar, K. V. Kheruntsyan, A. Aspect, D. Boiron, and C. I. Westbrook, *Phys. Rev. Lett.* **105**, 190402 (2010).
- [12] G. B. Partridge, J.-C. Jaskula, M. Bonneau, D. Boiron, and C. I. Westbrook, *Phys. Rev. A* **81**, 053631 (2010).
- [13] W. Vassen, C. Cohen-Tannoudji, M. Leduc, D. Boiron, C. I. Westbrook, A. Truscott, K. Baldwin, G. Birkl, P. Cancio, and M. Trippenbach, *Rev. Mod. Phys.* **84**, 175 (2012).
- [14] J. Estève, C. Gross, A. Weller, S. Giovanazzi, and M. K. Oberthaler, *Nature (London)* **455**, 1216 (2008).
- [15] C. Gross, T. Zibold, E. Nicklas, J. Estève, and M. K. Oberthaler, *Nature (London)* **464**, 1165 (2010).
- [16] M. F. Riedel, P. Böhi, Y. Li, T. W. Hänsch, A. Sinatra, and P. Treutlein, *Nature (London)* **464**, 1170 (2010).
- [17] R. Bücker, J. Grond, S. Manz, T. Berrada, T. Betz, C. Koller, U. Hohenester, T. Schumm, A. Perrin, and J. Schmiedmayer, *Nature Phys.* **7**, 608 (2011).
- [18] B. Lücke, M. Scherer, J. Kruse, L. Pezzé, F. Deuretzbacher, P. Hyllus, O. Topic, J. Peise, W. Ertmer, J. Arlt, L. Santos, A. Smerzi, and C. Klempt, *Science* **334**, 773 (2011).
- [19] E. M. Bookjans, C. D. Hamley, and M. S. Chapman, *Phys. Rev. Lett.* **107**, 210406 (2011).
- [20] V. Krachmalnicoff, J.-C. Jaskula, M. Bonneau, V. Leung, G. B. Partridge, D. Boiron, C. I. Westbrook, P. Deuar, P. Ziń, M. Trippenbach, and K. V. Kheruntsyan, *Phys. Rev. Lett.* **104**, 150402 (2010).
- [21] See Supplementary Material at <http://link.aps.org/supplemental/10.1103/PhysRevLett.108.260401> for a more detailed discussion of correlation functions, the correlation coefficient C , and simulation methods.
- [22] M. Schellekens, R. Hoppeler, A. Perrin, J. Viana Gomes, D. Boiron, A. Aspect, and C. I. Westbrook, *Science* **310**, 648 (2005).
- [23] S. S. Hodgman, R. G. Dall, A. G. Manning, K. G. H. Baldwin, and A. G. Truscott, *Science* **331**, 1046 (2011).
- [24] K. Mølmer, A. Perrin, V. Krachmalnicoff, V. Leung, D. Boiron, A. Aspect, and C. I. Westbrook, *Phys. Rev. A* **77**, 033601 (2008).
- [25] M. Ögren and K. V. Kheruntsyan, *Phys. Rev. A* **79**, 021606 (2009).
- [26] D. S. Petrov, G. V. Shlyapnikov, and J. T. M. Walraven, *Phys. Rev. Lett.* **87**, 050404 (2001).
- [27] P. Deuar *et al.* (to be published).
- [28] P. Deuar, J. Chwedeńczuk, M. Trippenbach, and P. Ziń, *Phys. Rev. A* **83**, 063625 (2011).
- [29] C. Su and K. Wódkiewicz, *Phys. Rev. A* **44**, 6097 (1991).
- [30] M. A. Rowe, D. Kielpinski, V. Meyer, C. A. Sackett, W. M. Itano, C. Monroe, and D. J. Wineland, *Nature (London)* **409**, 791 (2001).
- [31] H. Sakai *et al.*, *Phys. Rev. Lett.* **97**, 150405 (2006).
- [32] R. Lewis-Swan and K. V. Kheruntsyan (to be published).
- [33] J. G. Rarity and P. R. Tapster, *Phys. Rev. Lett.* **64**, 2495 (1990).

Violation of the Cauchy-Schwarz inequality with matter waves

 K. V. Kheruntsyan,* J.-C. Jaskula, P. Deuar, M. Bonneau, G. B. Partridge,
 J. Ruaudel, R. Lopes, D. Boiron, and C. I. Westbrook

*To whom correspondence should be addressed; E-mail: karen.kheruntsyan@uq.edu.au

Definitions of correlation functions. The second-order correlation function $\mathcal{G}^{(2)}(\mathbf{k}, \mathbf{k}')$ between the particle number densities at two points in momentum space is defined as

$$\mathcal{G}^{(2)}(\mathbf{k}, \mathbf{k}') = \langle : \hat{n}(\mathbf{k}) \hat{n}(\mathbf{k}') : \rangle = \langle \hat{a}^\dagger(\mathbf{k}) \hat{a}^\dagger(\mathbf{k}') \hat{a}(\mathbf{k}') \hat{a}(\mathbf{k}) \rangle. \quad (\text{S1})$$

Here, $\hat{a}(\mathbf{k})$ is the Fourier transform of the atomic field annihilation operator $\hat{\Psi}(\mathbf{x})$, and $\hat{n}(\mathbf{k}) = \hat{a}^\dagger(\mathbf{k}) \hat{a}(\mathbf{k})$ is the density operator corresponding to the atomic momentum distribution (with \mathbf{k} denoting the wave-vector $\mathbf{k} = m\mathbf{v}/\hbar$).

The normalized correlation functions shown in Fig. 2 of the main text are defined as

$$g_{\text{BB}}^{(2)}(\Delta\mathbf{k}) = \mathcal{G}_{\text{BB}}^{(2)}(\Delta\mathbf{k}) / \int_{\mathcal{V}} d^3\mathbf{k} \langle \hat{n}(\mathbf{k}) \rangle \langle \hat{n}(-\mathbf{k} + \Delta\mathbf{k}) \rangle, \quad (\text{S2})$$

and

$$g_{\text{CL}}^{(2)}(\Delta\mathbf{k}) = \mathcal{G}_{\text{CL}}^{(2)}(\Delta\mathbf{k}) / \int_{\mathcal{V}} d^3\mathbf{k} \langle \hat{n}(\mathbf{k}) \rangle \langle \hat{n}(\mathbf{k} + \Delta\mathbf{k}) \rangle. \quad (\text{S3})$$

The normalization ensures that for uncorrelated densities $g_{\text{BB}}^{(2)}(\Delta\mathbf{k}) = 1$ and $g_{\text{CL}}^{(2)}(\Delta\mathbf{k}) = 1$.

These functions are shown in Fig. 2 of the main text. The widths and amplitudes of the BB and CL correlation functions are measured using Gaussian fits to their cuts through the centre of the 2D surface plots along the k_z and k_{xy} axis; the fits and the data are shown in Fig. S1 (same data as in Fig. 2 of the main text but with error bars).

CS violation and correlation widths. A fair understanding of the dependence of the multimode CS violation C on the correlation functions can be gained from a simple model, which is readily related to the experimental data. Let us make several assumptions: (A) a Gaussian shape for the normalized correlation functions (those shown in Fig. 2 of the main text):

$$g_{\text{CL/BB}}^{(2)}(\Delta\mathbf{k}) = 1 + h_{\text{CL/BB}} \prod_d e^{-\Delta k_d^2 / 2\sigma_{\text{CL/BB},d}^2}, \quad (\text{S4})$$

where CL and BB are the two kinds of correlations, the index $d = x, y, z$ runs over spatial directions, $\sigma_{\text{CL/BB},d}$ are standard deviations (correlation lengths, in wave-number units) of the correlation peak, and $h_{\text{CL/BB}}$ are the peak heights above the background level of unity. Let us further assume (B) that the counting zones \mathcal{V}_i are much broader than the relevant correlation lengths in all directions. This allows us to neglect boundary effects caused by atom pairs in which one member

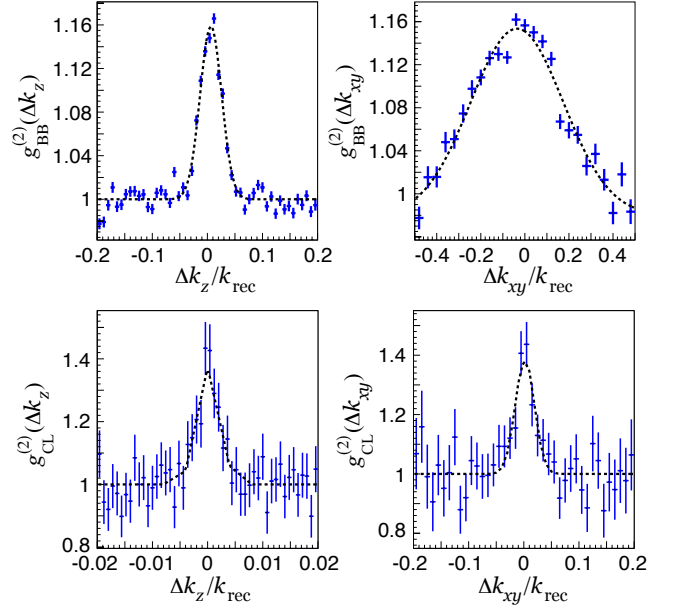


Figure S1. Central cuts of the BB and CL correlation functions, $g_{\text{BB}}^{(2)}(\Delta\mathbf{k})$ and $g_{\text{CL}}^{(2)}(\Delta\mathbf{k})$, along the k_z and k_{xy} axis.

lies just inside the zone and the other just outside [1]. Finally, for simplicity we assume (C) that the halo density in the relevant regions is constant: $\langle \hat{n}(\mathbf{k} + \Delta\mathbf{k}) \rangle = \bar{n}$, and (D) that the two counting zones have the same widths in each direction d , hence the same overall momentum-space volumes $\mathcal{V}_1 = \mathcal{V}_2 \equiv \mathcal{V}$.

With these assumptions, the integrated correlation functions are

$$\bar{g}_{ii}^{(2)} \approx \bar{n}^2 \mathcal{V} \left\{ \mathcal{V} + h_{\text{CL}} (2\pi)^{3/2} \prod_d \sigma_{\text{CL},d} \right\} \quad (\text{S5})$$

($i = 1, 2$) and

$$\bar{g}_{12}^{(2)} \approx \bar{n}^2 \mathcal{V} \left\{ \mathcal{V} + h_{\text{BB}} (2\pi)^{3/2} \prod_d \sigma_{\text{BB},d} \right\}, \quad (\text{S6})$$

where the counting zones \mathcal{V}_1 and \mathcal{V}_2 are non-overlapping. Taking the widths of the counting zones \mathcal{V} as L_d , the next order corrections are $\sim \mathcal{O}(\sum_d \frac{\sigma_{\text{CL/BB},d}}{L_d})$ with respect to the terms proportional to $h_{\text{CL/BB}}$, and so are negligible due to our assumption (B).

It is useful to define an effective geometric mean correlation width

$$\bar{\sigma}_{\text{CL/BB}}^3 = \prod_d \sigma_{\text{CL/BB},d}. \quad (\text{S7})$$

The large counting volume assumption (B) means $\bar{\sigma}_{\text{CL/BB}}/\mathcal{V}^{1/3} \ll 1$, and taking leading order terms in this small parameter, we use Eqs. (S5–S6) to obtain an estimate for the CS violation between opposite zones:

$$C \approx 1 + \frac{(2\pi)^{3/2}}{\mathcal{V}} [h_{\text{BB}} \bar{\sigma}_{\text{BB}}^3 - h_{\text{CL}} \bar{\sigma}_{\text{CL}}^3]. \quad (\text{S8})$$

Now it is clear that nonclassical measurements ($C > 1$) can still occur for a back-to-back correlation peak lower than the collinear one, provided that the coherence volume for the back-to-back pairs is correspondingly larger and that it still fits inside our counting volumes \mathcal{V} . Expression (S8) also hints that a maximally large CS violation will occur when the counting volumes are of about the same size as the coherence volumes, since the excursion above one is proportional to the ratios $\bar{\sigma}_{\text{CL/BB}}^3/\mathcal{V}$.

CS violation and the number of zones M . To apply the above model to our experiment, we take the radial (r) width of the counting zone L_r to be approximately equal to the width w_r of the scattering sphere in the radial direction, $L_r \approx w_r$. Also, the zone size is $L_z = k_{\text{rec}}/8$ in the longitudinal z direction (where we recall that the analyzed part of the scattering sphere corresponds to $|k_z| < 0.5k_{\text{rec}}$, which is further cut into 8 polar zones), and $L_c \approx 2\pi k_{\text{rec}}/(M/8)$ along the circumference of the ring in the xy plane. With this,

$$C \approx 1 + M \frac{\sqrt{2\pi}}{w_r k_{\text{rec}}^2} [h_{\text{BB}} \bar{\sigma}_{\text{BB}}^3 - h_{\text{CL}} \bar{\sigma}_{\text{CL}}^3] \quad (\text{S9})$$

This is a linear growth with M .

The width of a single zone along the circumference, L_c , becomes comparable with, or narrower than, the measured correlation width $\sigma_{\text{BB},xy} \approx 0.21k_{\text{rec}}$ when $M \gtrsim 150$. This is indeed when we start to see a deviation from the linear behaviour in Fig. 3 of the main text.

For large M , the zones are narrow along the circumference, so that the broad zone assumption (B) does not hold, and variation of Δk along this direction does not change the correlation from its peak value. If one carries out the calculation again, but with an alternative assumption (B') that the counting zone is now much *narrower* than the correlation widths $\sigma_{\text{CL/BB},d}$, the estimate of C becomes

$$C \approx 1 + \frac{32\pi}{w_r k_{\text{rec}}} [h_{\text{BB}} \sigma_{\text{BB},z} \sigma_{\text{BB},xy} - h_{\text{CL}} \sigma_{\text{CL},z} \sigma_{\text{CL},xy}], \quad (\text{S10})$$

which amounts to a replacement of one set of Gaussian widths $\sigma_{\text{CL/BB},xy}$ by $L_c/\sqrt{2\pi}$. The correlation coefficient C reaches a saturation value that does not depend on M at all, but may be larger or smaller than unity, depending on how the widths

and heights play out. In our case it is still a violation, with $C > 1$.

If the zones \mathcal{V} were made narrower in all directions than the corresponding correlation widths, we would recover the two-mode expression

$$C \approx \frac{h_{\text{BB}} + 1}{h_{\text{CL}} + 1}. \quad (\text{S11})$$

In our case, since $h_{\text{BB}} < h_{\text{CL}}$, this would not be a CS violation anymore.

Finally, when one considers non-opposite zones, such as the lower experimental data in Fig. 3 of the main text, the value of h_{BB} tends to zero as there is no pairing. In this case, the expressions (S9) and (S10) show that C will lie always slightly below unity for large counting zones. For the small-counting-zone limit, $C \rightarrow 1/g_{\text{CL}}^{(2)}(0)$. In neither case can there be CS violation.

Stochastic Bogoliubov simulations. The theoretical results shown in Fig. 3 of the main text come from numerical simulations using the positive- P Bogoliubov method, which is described in detail in Ref. [2]. It was used previously for our experiment in Refs. [1, 3]. In a nutshell, we evolve the system in a time-dependent Bogoliubov approximation, taking the condensate part at time t as the solution of the Gross-Pitaevskii mean field evolution equation for the colliding condensates. The numerical lattice required to describe this model is too large for a direct solution of the Bogoliubov-de Gennes equations to be tractable, so the fluctuation field (which is responsible for the scattered halo) is represented instead using the positive- P representation. This leads to coupled linear stochastic differential equations which *can* be integrated numerically. The ensemble of such stochastic realisations corresponds to the full Bogoliubov dynamics, and allows one to estimate observables to within a well defined statistical accuracy.

Simulations were carried out for a collision of metastable $^4\text{He}^*$ atoms in the $m_F = 0$ state (with the s -wave scattering length of $a = 5.3$ nm) for several initial total number of atoms, $N = 50\,000$, $85\,000$, and $110\,000$ (the actual value in the experiment fluctuates from shot to shot in the vicinity of $\sim 10^5$). The atoms were assumed to be trapped initially in the $m_F = 1$ state in a harmonic trapping potential with frequencies $\omega_z/2\pi = 7.5$ Hz and $\omega_x/2\pi = \omega_y/2\pi = 1500$ Hz.

To begin with, several initial states were tried: a zero-temperature ($T = 0$) Bose-Einstein condensate (BEC), and $T > 0$ quasicondensates in elongated 3D traps with phase coherence lengths of $l_\phi = 45$ μm and $l_\phi = 100$ μm (taken as a half-width-at-half-maximum of the first-order correlation function $g^{(1)}(0, z)$ from the center of the trap in the longitudinal direction), which are in the range expected for the cloud in the experiment. For comparison, the longitudinal size of the initial cloud along z is about 980 μm .

The magnitude of the calculated C at long times differed by at most 0.007 between the simulations with quasicondensate and BEC initial conditions (see Fig. S2). Since this is a

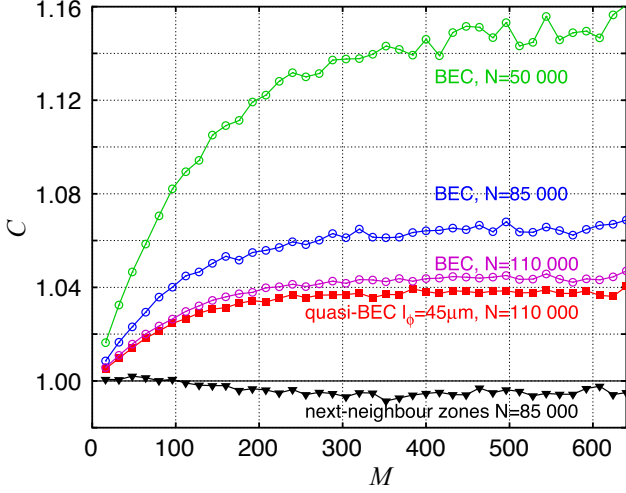


Figure S2. Calculated correlation coefficient C as a function of the number of zones M at the end of the simulation ($t = 186 \mu\text{s}$ for the $N = 110\,000$ atom simulations, $248 \mu\text{s}$ for the others). Circles are for C between opposite zones and BEC initial conditions; squares similarly, but with a quasicondensate initial condition having the shortest phase coherence length $l_\phi = 45 \mu\text{m}$. Filled triangles show C between next-neighbour zones, which do not violate the CS inequality ($C < 1$), as expected. One sees that the value of C depends strongly on N , while its shape as a function of M is almost unchanged.

very small effect on C in comparison with the effect of particle number (or in comparison with the effect on the shape of correlation functions), we will consider mainly the BEC initial conditions in what follows. The simulation of quasicondensates with a Bogoliubov description, in which the initial $T > 0$ states were based on the description of Petrov *et al.* [4] for elongated 3D clouds, will be described in a future work [5].

Theoretical predictions for C . The simulation data in Fig. 3 of the main text are for a time of $248 \mu\text{s}$ after the start of the collision with $85\,000$ atoms, which we regard as the best-fit value of N .

The values of the correlation coefficient at the end of simulations for various atom numbers and initial conditions are shown in Fig. S2. The time evolution of its saturation value at large M [i.e., small counting volumes as per Eq. (S10)] is shown in Fig. S3(b), along with the time evolution of the overall number of scattered atoms [Fig. S3(a)]. It is seen that the magnitude of C depends strongly on the initial number of atoms N , while its shape as a function of M remains almost unchanged. In particular, small N and hence small number of scattered particles in the halo, N_{sc} [see Fig. S3(a)] correspond to large values of C for a given counting zone size. This can be roughly understood from a simple two-mode model of standard spontaneous parametric down-conversion in the undepleted pump approximation [6], with a Hamiltonian $\hat{H} \sim \hat{a}_1^\dagger \hat{a}_2^\dagger + \text{h.c.}$ that produces atom pairs in the a_1 and

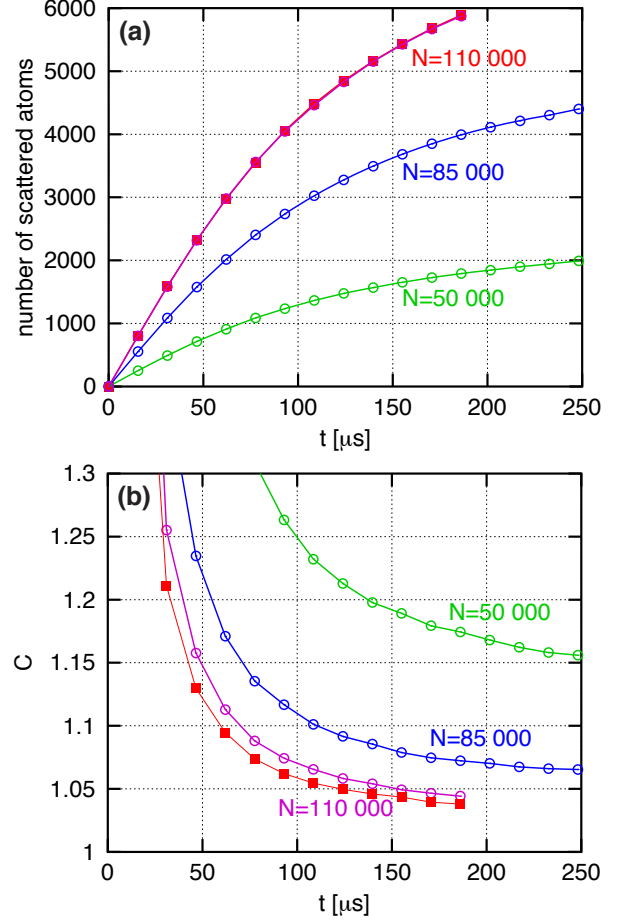


Figure S3. Calculated time evolution. Panel (a) shows the number of scattered atoms as a function of time for various initial atom numbers N . Panel (b) shows the saturation mean value of C at large M between opposite zones – the value is averaged over $M \geq 400$. In both panels, circles are for BEC initial conditions, squares for the $l_\phi = 45 \mu\text{m}$ quasicondensate as in Fig. S2. The $C(M)$ data in Fig. 3 of the main text and in Fig. S2 here are for the last times shown here. One sees that at that moment C has already achieved its long-time value, or is very close to it.

a_2 modes. This is a process similar to the one that occurs during our condensate collision. In this toy model, the BB correlation analogue is $g_{12}^{(2)} = 2 + 1/n$ [7], where n is the mean particle number in modes a_1 and a_2 ($n_1 = n_2 \equiv n$), and the CL correlation analogue is $g_{11}^{(2)} = g_{22}^{(2)} = 2$. Hence, $C \approx 1 + 1/2n$ in this model, showing a similar scaling with atom number to our simulations. Resorting to this toy model is done only for qualitative understanding of the scaling of C with N_{sc} and hence with the number of atoms in a given counting zone. The quantitative aspects of the model, however, are too crude to be applicable to our system due to the rapid changes in the “pump” (source condensate) density profile, which is in sharp contrast to the undepleted, i.e., *constant* in time, pump approximation.

The experimental values in Fig. 3 of the main text come from an average over many realizations with different atom

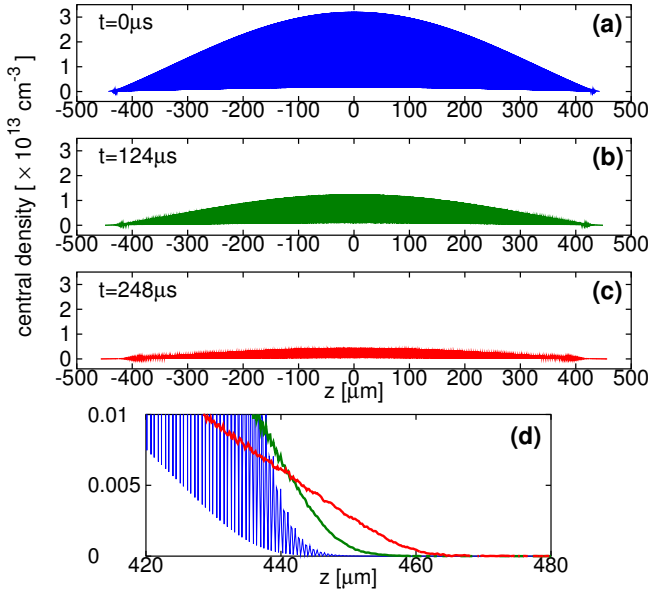


Figure S4. Central density along z (at $x = y = 0$) of the two colliding condensates, for the total initial number of atoms $N = 85,000$, shown at three different times: $t = 0$ – (a), $t = 124 \mu\text{s}$ – (b), and $t = 248 \mu\text{s}$ – (c). The overlap region includes the interference fringes, which are, however, not visible on this scale due to the high frequency of the modulation. As we see, the peak density at $t = 248 \mu\text{s}$ is reduced by a factor of ~ 7 due to the rapid expansion of the condensates in the transverse dimensions, which is the main reason for the collision to cease. Panel (d) shows detail at the cloud edges.

numbers N from shot to shot. However, the contribution of small-atom-number shots (which would have a high magnitude of C , and poor signal-to-noise) to the atom-number fluctuations that go into the calculation of C is small. Taking this into account, and noting that $N \approx 85,000$ is the most typical value, best agreement between this value and experiment is very reasonable.

The time evolution in Fig. S3 shows that, at the final simulation times shown in Fig. 3 of the main text and Fig. S3 here, the correlation coefficient C is already at, or very close to, its long-time value. The maximum simulation time is the result of a trade-off between computational efficiency and accuracy — the size of the numerical grid required to encompass the clouds grows rapidly with longer times. Even though our maximum simulation time is appreciably shorter than the time it takes for the clouds to move completely past each other along z (about 5 ms), the production of halo particles is already strongly saturating by the end of the simulation [see Fig. S3(a)]. This is due to a rapid loss of central density of the colliding source BECs because of their expansion perpendicular to the long (collision) axis. In other words, the end of collision and the saturation in the number of scattered atoms in Fig. S3(a) is determined not by a geometric consideration (i.e., a complete spatial separation of the colliding BECs along z), but by the rapid loss of peak density (see Fig. S4) due to the expansion in the transverse direction. The pair production rate is roughly proportional to the integral of density squared

[8], which is the reason for the premature cessation of particle scattering, and allows relatively short simulation times to be considered adequate.

Cauchy-Schwarz inequality and sub-Poissonian number imbalance. The strength of correlation between the atom number fluctuations in two diametrically opposite zones on the collision halo can also be characterised via a normalised variance [1]

$$V = \frac{\langle [\Delta(\hat{N}_1 - \hat{N}_2)]^2 \rangle}{\langle \hat{N}_1 \rangle + \langle \hat{N}_2 \rangle}, \quad (\text{S12})$$

which can be rewritten in terms of the second-order correlation functions,

$$V = 1 + \frac{\bar{\mathcal{G}}_{11}^{(2)} + \bar{\mathcal{G}}_{22}^{(2)} - 2\bar{\mathcal{G}}_{12}^{(2)} - (\langle \hat{N}_1 \rangle - \langle \hat{N}_2 \rangle)^2}{\langle \hat{N}_1 \rangle + \langle \hat{N}_2 \rangle}. \quad (\text{S13})$$

The variance is normalised to the level of uncorrelated, Poissonian fluctuations and $V < 1$ implies sub-Poissonian statistics of the relative number imbalance. From this we see that the relationship between sub-Poissonian number imbalance and the violation of the CS inequality is especially transparent in the symmetric case of $\langle \hat{N}_1 \rangle = \langle \hat{N}_2 \rangle$, in which case stronger-than-classical correlation, $\bar{\mathcal{G}}_{12}^{(2)} > [\bar{\mathcal{G}}_{11}^{(2)} \bar{\mathcal{G}}_{22}^{(2)}]^{1/2}$ (in the sense of CS violation), follows from $V < 1$ and hence represents a necessary condition for sub-Poissonian statistics. This last assertion follows from the fact that, if $V < 1$ and $\langle \hat{N}_1 \rangle = \langle \hat{N}_2 \rangle$, then one must have $\bar{\mathcal{G}}_{12}^{(2)} > \frac{1}{2}(\bar{\mathcal{G}}_{11}^{(2)} + \bar{\mathcal{G}}_{22}^{(2)})$, where $\frac{1}{2}(\bar{\mathcal{G}}_{11}^{(2)} + \bar{\mathcal{G}}_{22}^{(2)}) \geq [\bar{\mathcal{G}}_{11}^{(2)} \bar{\mathcal{G}}_{22}^{(2)}]^{1/2}$, and therefore $\bar{\mathcal{G}}_{12}^{(2)} \geq [\bar{\mathcal{G}}_{11}^{(2)} \bar{\mathcal{G}}_{22}^{(2)}]^{1/2}$. The opposite is, however, not true in general, because having $\bar{\mathcal{G}}_{12}^{(2)} > [\bar{\mathcal{G}}_{11}^{(2)} \bar{\mathcal{G}}_{22}^{(2)}]^{1/2}$ does not necessarily guarantee $V < 1$, unless $\bar{\mathcal{G}}_{11}^{(2)} = \bar{\mathcal{G}}_{22}^{(2)}$. Thus, violation of the CS inequality and sub-Poissonian number imbalance are equivalent only in the completely symmetric case of $\langle \hat{N}_1 \rangle = \langle \hat{N}_2 \rangle$ and $\bar{\mathcal{G}}_{11}^{(2)} = \bar{\mathcal{G}}_{22}^{(2)}$.

We emphasise, however, that the equivalence of the CS violation and the relative number imbalance in the symmetric case (or the expected ‘approximate equivalence’ in the nearly symmetric case, as is the case in our experiment) is only of qualitative nature. The quantitative relationship between the strength of the CS violation and the degree of suppression of V below the Poissonian level of fluctuations can, on the other hand, be very different if we analyse these as functions of the zone size or the number of zones M into which we cut the scattering halo. Indeed, as was demonstrated in Ref. [1], strong suppression of V below unity is observed for the broader zones (see Fig. 3 of [1]) – a situation in which the CS inequality is only marginally violated as seen from Fig. 3 of the main text at small M . Conversely, the CS inequality is maximally violated for large M (smaller zone sizes), in which case the variance V is almost indistinguishable from the Poissonian shot-noise level of $V = 1$. This difference highlights

the importance of quantifying any particular type of quantum correlations in an operationally defined manner.

-
- [1] J.-C. Jaskula, M. Bonneau, G. B. Partridge, V. Krachmalnicoff, P. Deuar, K. V. Kheruntsyan, D. Boiron, A. Aspect, and C. I. Westbrook, *Phys. Rev. Lett.* **105**, 190402 (2010).
- [2] P. Deuar, J. Chwedeńczuk, M. Trippenbach, and P. Ziń, *Phys. Rev. A* **83**, 063625 (2011).
- [3] V. Krachmalnicoff, J.-C. Jaskula, M. Bonneau, V. Leung, G. B. Partridge, D. Boiron, C. I. Westbrook, P. Deuar, P. Ziń, M. Trippenbach, and K. V. Kheruntsyan, *Phys. Rev. Lett.* **104**, 150402 (2010).
- [4] D. S. Petrov, G. V. Shlyapnikov, and J. T. M. Walraven, *Phys. Rev. Lett.* **87**, 050404 (2001).
- [5] P. Deuar *et al.*, in preparation.
- [6] D. F. Walls and G. J. Milburn, *Quantum Optics*, 2nd ed. (Springer, Berlin, 2008).
- [7] C. M. Savage, P. E. Schwenn, and K. V. Kheruntsyan, *Phys. Rev. A* **74**, 033620 (2006).
- [8] A. Perrin, C. M. Savage, D. Boiron, V. Krachmalnicoff, C. I. Westbrook, and K. V. Kheruntsyan, *New J. Phys.* **10**, 045021 (2008).